OXFORD

Research Article

The orientation of a decellularized uterine scaffold determines the tissue topology and architecture of the regenerated uterus in rats[†]

Fumie Miki[1], Tetsuo Maruyama [1,*], **Kaoru Miyazaki** [1]**, Tomoka Takao[1],
Yushi Yoshimasa** [1]**, Satomi Katakura[1], Hanako Hihara[1], Sayaka Uchida[1],
Hirotaka Masuda[1], Hiroshi Uchida[1], Toshihiro Nagai[2],
Shinsuke Shibata** [2] **and Mamoru Tanaka** [1]

[1]Department of Obstetrics and Gynecology, Keio University School of Medicine, Tokyo, Japan and [2]Electron Microscope Laboratory, Keio University School of Medicine, Tokyo, Japan

*Correspondence: Department of Obstetrics and Gynecology, Keio University School of Medicine, 35 Shinanomachi, Shinjuku-ku, Tokyo 160-8582, Japan. Tel: +81 3 5363 3578; Fax: +81 3 5363 3578; E-mail: tetsuo@keio.jp

Abstract

A decellularized uterine scaffold (DUS) prepared from rats permits recellularization and regeneration of uterine tissues when placed onto a partially excised uterus and supports pregnancy in a fashion comparable to the intact uterus. The underlying extracellular matrix (ECM) together with an acellular, perfusable vascular architecture preserved in DUS is thought to be responsible for appropriate regeneration of the uterus. To investigate this concept, we examined the effect of the orientation of the DUS-preserving ECM and the vascular architecture on uterine regeneration through placement of a DUS onto a partially defective uterine area in the reversed orientation such that the luminal face of the DUS was outside and the serosal face was inside. We characterized the tissue structure and function of the regenerated uterus, comparing the outcome to that when the DUS was placed in the correct orientation. Histological analysis revealed that aberrant structures including ectopic location of glands and an abnormal lining of smooth muscle layers were observed significantly more frequently in the reversed group than in the correct group (70% vs. 30%, $P < 0.05$). Despite the changes in tissue topology, the uteri regenerated with an incorrectly oriented DUS could achieve pregnancy in a way similar to uteri regenerated with a correctly oriented DUS. These results suggest that DUS-driven ECM orientation determines the regenerated uterus structure. Using DUS in the correct orientation is preferable when clinically applied. The disoriented DUS may deteriorate the tissue topology leading to structural disease of the uterus even though the fertility potential is not immediately affected.

Summary Sentence

The disoriented placement of a decellularized uterine scaffold onto a partially defective uterine area results in the regeneration of uterus with aberrant structures including ectopic location of glands and an abnormal lining of smooth muscle layers in rats.

Key words: uterus, decellularization, scaffold, topology, extracellular matrix.

Introduction

Structural abnormalities and dysfunctional tissues of the uterus can cause female infertility. The absence of the uterus due to congenital uterine malformation and hysterectomy results in absolute infertility. Gestational surrogacy or uterine transplantation enables women with absolute uterine infertility to achieve genetic parenthood [1–3]. However, many obstacles can be encountered with these approaches, including cost, the health of the surrogate mother and complex ethical, medical and legal issues regarding uterine transplantation as well as societal issues and the attitudes regarding donors and recipients [4–8]. As an alternative therapeutic strategy to overcome these difficulties, a bioartificial uterus has recently emerged, incorporating both uterine architecture and/or appropriate cellular constituents [8, 9]. Among the procedures for organ and tissue bioengineering, perfusion decellularization has been employed as a novel technology to generate native extracellular matrix (ECM) scaffolds with intact 3D anatomical architecture and vasculature. This is achieved through detergent- or high hydrostatic pressure-mediated removal of cell components [10]. Indeed, several groups including ours have attempted exploratory uterine bioengineering using a decellularized scaffold (DS) prepared from the uterus of rodents and pigs in which the cellular components of the uterus are completely depleted by various methodologies, such as anionic detergent or high hydrostatic pressure [11–16].

A key advantage of the DS-based methodology is its ability to preserve elements of the tissue-specific ECM and 3D architecture, providing crucial cues for cell engraftment in vivo as well as in vitro [10, 17]. This is explained by the fact that the ECM directly determines cellular responses, including proliferation, differentiation, and migration [18, 19]. Rat DS prepared from uteri [decellularized uterine scaffold (DUS)] can support the recellularization and regeneration of rat uterine tissues when placed onto a partially excised uterus, permitting pregnancy nearly comparable to that achieved with an intact uterus [11, 12, 15]. However, it remains to be elucidated how the DUS, i.e., the uterus-specific ECM, controls the regeneration and tissue organization of the uterus. Defining the mechanism(s) underlying the function of a DUS will provide clues about how DUS patches should be handled when used in regenerative medicine for women with uterine factor infertility.

The uterus is a unique organ that cyclically and repeatedly undergoes structural and functional changes to prepare for the acceptance of embryos and to subsequently maintain pregnancy throughout the reproductive period. The unique properties of the uterus, including the cyclic and potent regenerative capacity of endometrium, is at least in part attributable to stem cell systems present in the uterus [20, 21]. For instance, single-cell suspensions of human endometrial cells, even putative human endometrial stem/progenitor cells, are able to give rise to endometrium-like tissue containing well-delineated glandular structures without any assistance of exogenous ECM or scaffold when they are transplanted under the kidney capsule followed by treatment with ovarian steroid hormones [22–24]. These data suggest the presence of potent self-regenerative and self-organizing abilities in uterine cells themselves. It is intriguing to investigate how uterine endometrial cells interact with a DUS.

Here, we addressed how the DUS-preserving ECM and 3D architecture directs the regeneration of the uterus. Thus, we have investigated the effect of DUS orientation on uterine regeneration through the placement of DUS patches on partially defective uterine areas in a reversed orientation such that the luminal face of the DUS was outside and the serosal face was inside. We characterized the resultant tissue structure and function of the regenerated uterus, comparing the outcome to those placed with the DUS in the correct orientation.

Materials and methods

Collection of rat organ and tissue samples

Female Sprague-Dawley (SD) rats (9 weeks old) weighing 190–230 g were obtained from Oriental Yeast (Tokyo, Japan). The rats were kept on a constant dark/light cycle (12 h each) and given standard rat chow and water ad libitum. They were anesthetized with isoflurane. The anterior abdominal wall was opened longitudinally along the midline, and the uterus together with its accompanying arteries and veins were excised as previously described [11]. Small intestines were also obtained from adult SD rats euthanized under general anesthesia. All animals were cared for in accordance with the rules and regulations set out by Keio University School of Medicine for Animal Care. Animal protocols were approved by the Laboratory Animal Center of the Keio University School of Medicine. Rats were euthanized under general anesthesia.

Decellularization of the uterus and small intestine

Decellularization of rat uteri was performed according to the previously described protocol [11]. In brief, uteri were washed with PBS overnight through perfusion via the aorta using a peristaltic pump (Atto, Tokyo, Japan). The uterus was then perfused with SDS (Wako, Japan), an anionic detergent, in distilled water (DW) for 72 h starting with 0.01% (wt/vol) SDS for 24 h and then with 0.1% (wt/vol) SDS for 24 h at 4°C and with 1% (wt/vol) SDS for 24 h at room temperature. Subsequently, the uterus was washed with DW for 15 min and 1% Triton X-100 (Sigma) for 30 min to remove residual SDS. The DUS was washed extensively with sterile PBS and stored in PBS containing a 1% antibiotic and antimycotic solution (Sigma) at 4°C for up to 1 week.

Small intestines were washed in PBS to completely remove intestinal contents and cut into 15-mm long fragments. These fragments were immersed in increasing SDS concentrations (0.01%, 0.1%, and 1%) for 24 h each. Then, samples were rinsed in DW for 15 min and immersed in 1% Triton X-100 (Sigma) for 30 min. All protocols were performed on a shaker set at a frequency of 1 Hz. The decellularized small intestine scaffold (DSIS) was washed extensively with sterile PBS and stored in PBS containing 1% antibiotic and antimycotic solution at 4°C for up to 1 week.

Histological and immunofluorescence analyses

For permanent preparations, uterine and small intestine tissues for histological analysis were fixed in 4% paraformaldehyde (PFA) and embedded in paraffin blocks. For deparaffinization, the slides were submerged twice in 100% xylene for 5 min, twice in 100% ethanol for 3 min, in 90% ethanol for 3 min, in 80% ethanol for 3 min, and in 70% ethanol for 3 min. Deparaffinized slides were subjected to hematoxylin and eosin (H&E) staining or Masson's trichrome (MT) staining in which collagen fibers, nuclei, and smooth muscle layer were stained blue, purple, and red, respectively. H&E and MT staining was carried out as described previously [11].

For immunofluorescence staining, uterine and small intestine tissues were embedded in Tissue-Tek optimum cutting temperature (O.C.T.) compound (Sakura Finetek, Inc., Torrance, CA), frozen, and sectioned at a thickness of 7 μm. Cryosections were transferred to microscope slides, air-dried for 30 min, and washed twice in PBS for 3 min. Sections were fixed in 4% PFA for 10 min at room temperature and permeabilized with 0.1% Triton X-100 in PBS for 10 min. After blocking with 1% BSA/PBS, tissue sections were incubated with the pre-titrated primary antibodies for 120 min. Primary antibodies including mouse monoclonal anti-cytokeratin (Dako), mouse monoclonal anti-smooth muscle actin (Dako), and mouse monoclonal anti-desmin (Dako) antibodies were used (1:100 dilution). Rabbit monoclonal anti-vitronectin (Abcam), rabbit polyclonal anti-fibronectin (Gene Tex), rabbit monoclonal anti-collagen Type IV (Rockland), rabbit monoclonal anti-collagen Type V (Rockland), rabbit polyclonal anti-collagen Type I (Abcam), and rabbit polyclonal anti-laminin (Thermo Fisher Scientific) antibodies were used (1:100 dilution) as primary antibodies to detect ECM proteins. Rabbit monoclonal anti-estrogen receptor-alpha (anti-ESR1, Abcam) and mouse monoclonal anti-progesterone receptor (anti-PGR, Thermo Fisher Scientific) were used (1:100 dilution) as primary antibodies to detect ovarian steroid hormone receptors. With regard to the negative control, we employed the same isotype antibodies: mouse monoclonal control antibody (Cell Signaling Technology) and rabbit monoclonal control antibody (Cell Signaling Technology).

The primary antibodies were visualized by incubation with anti-mouse or anti-rabbit IgG Alexa Flour 488 (Thermo Fisher Scientific) for 60 min as a secondary antibody (1:250 dilution). After nuclear staining with 1 mg/mL Hoechst 33342 (Thermo Fisher Scientific) for 10 min, the slides were washed and mounted with Fluoromount (DBS/Beckman Coulter). Each step was performed at room temperature. To quantify desmin expression, fluorescence intensities from images of five randomly selected microscopic fields of cells were semi-quantitatively analyzed by densitometry (Image J software, NIH Image).

Partial excision of the uterus and DUS placement

The rats underwent segmental excision of both uterine horns and were subjected to placement of a DUS patch onto the partially defective uterine area as previously described [11]. In brief, a segment approximately 1.5 cm in length and 1/2 of the total circumference was excised from one horn of the uterus, and the mesometrium was retained. The DUS was cut into small pieces (1.5 cm $\times$ 0.5 cm) and sutured in place with 6-0 Prolene sutures to replace the excised segment [11]. In this study, we marked the luminal side of the DUS patches with 6-0 PROLENE sutures. We placed and fixed the marked DUS patches with 6-0 PROLENE onto the partially defective area of the right uterine horn in the correct orientation and onto the left horn in reversed orientation in which the luminal side of the DUS was outside and the serosal side was inside. A DISIS was placed with its luminal face inside and fixed onto the partially defective areas of both uterine horns. The DUS- or DSIS-patched uteri were excised and subjected to histological, immunofluorescence, ultrastructural, and real-time PCR analyses 8 weeks after DUS placement.

The regenerated uterine horns were also assessed for their fertility. The DUS- or DSIS-treated rats were mated with male SD rats 8 weeks after the surgery. Fertilization was confirmed by the presence of a vaginal plug. They were euthanized 20 days after the presence of a vaginal plug, and uterine horns were examined for the number and weight of fetuses and excised for immunofluorescence analysis.

Real-time PCR

Total RNA was extracted from tissues using TRIZOL reagent (Thermo Fisher Scientific) according to the manufacturer's instructions. Total RNA was reverse transcribed into complementary DNA using ReverTra Ace qPCR RT kit (Toyobo) according to the manufacturer's instructions. progesterone receptor (*Pgr*) and glyceraldehyde-3-phosphate dehydrogenase (*Gapdh*) primers were synthesized with TaKaRa and estrogen receptor alpha (*Esr1*) primers were synthesized by Invitrogen. Primers used to amplify *Pgr*, *Esr1*, and *Gapdh* are as follows: *Pgr*, 5′-TTGCTTGCACGCTTGGAC-3′ and 5′-GGTATTGGCGAGACTACAGACGA-3′; *Esr1*, 5′-TTGCTCTTGGACAGGAAT-3′ and 5′-GGTTCATCATCATGCGGAATC-3′; *Gapdh*, 5′-GGCACAGTCAAGGCTGAGAATG-3′ and 5′-ATGGTGGTGAAGACGCCAGTA-3′. Real-time PCR was performed with the CFX 96 real-time PCR analysis system (Bio Rad) using SYBR Premix Ex Taq II (TaKaRa). *Gapdh* was amplified in parallel in each run as an internal control. PCR was performed for 40 cycles under the following conditions: denaturation at 95°C for 30 s; annealing at 95°C for 5 s; and extension at 61.5°C for 30 s. A melting curve was generated at the end of every run to ensure product uniformity (65°C to 95°C increment 0.5°C for 5 s). The relative amount of mRNA expression is shown as the mean $\pm$ SE.

Scanning electron microscopy (SEM) and transmission electron microscopy (TEM)

Decellularized uterine samples were fixed in 2.5% glutaraldehyde and washed with 0.1 M HEPES buffer (pH 7.4), followed by post-fixation with 1% osmium tetroxide (OsO_4). The samples were dehydrated with 50, 70, 80, 90, and 100% ethanol. Resin was permeated into the tissue using QY-1 (n-butyl glycidyl ether), and the samples were embedded with plain resin and polymerized. The resin blocks were semi-thin sectioned at 1.5 μm with diamond knives using an ultra-microtome (EM UC7; Leica) and stained with 0.5% toluidine blue. The blocks were ultra-thin sectioned at 70 nm with a diamond knife using the same ultra-microtome and sections were placed on copper grids. They were rinsed and then stained with 2% uranyl acetate, and then rinsed with DW followed by secondary stain with a lead citrate. The grids were observed with a transmission electron microscope (JEMM-1400Plus; JEOL Ltd) at an acceleration voltage of 80 kV.

Statistics

Statistical analysis was carried *out using* Statistical Package for the Social Sciences (SPSS) ver. 23 (SPSS Inc., Chicago, IL, USA). Results are expressed as means $\pm$ SEM. The Fisher exact test was used for categorized variables. All parameters were compared by one-way analysis of variance (ANOVA); if the means of the three populations were not considered to be equal, we followed up with a post-hoc test (Tukey's honestly significant difference test and Games-Howell test). *P* values less than 0.05 were considered statistically significant.

Results

Preparation and characterization of rat DUS

We first prepared DUSs from rat uterus using perfusion with SDS through the aorta as described previously [11]. Supplementary Figure S1A shows the gross findings of the uterus before and after decellularization (BD and AD, respectively). Both cell nuclei and cytoplasmic components were present in the rat uterus before decellularization (Supplementary Figure S1B and C, BD) but were
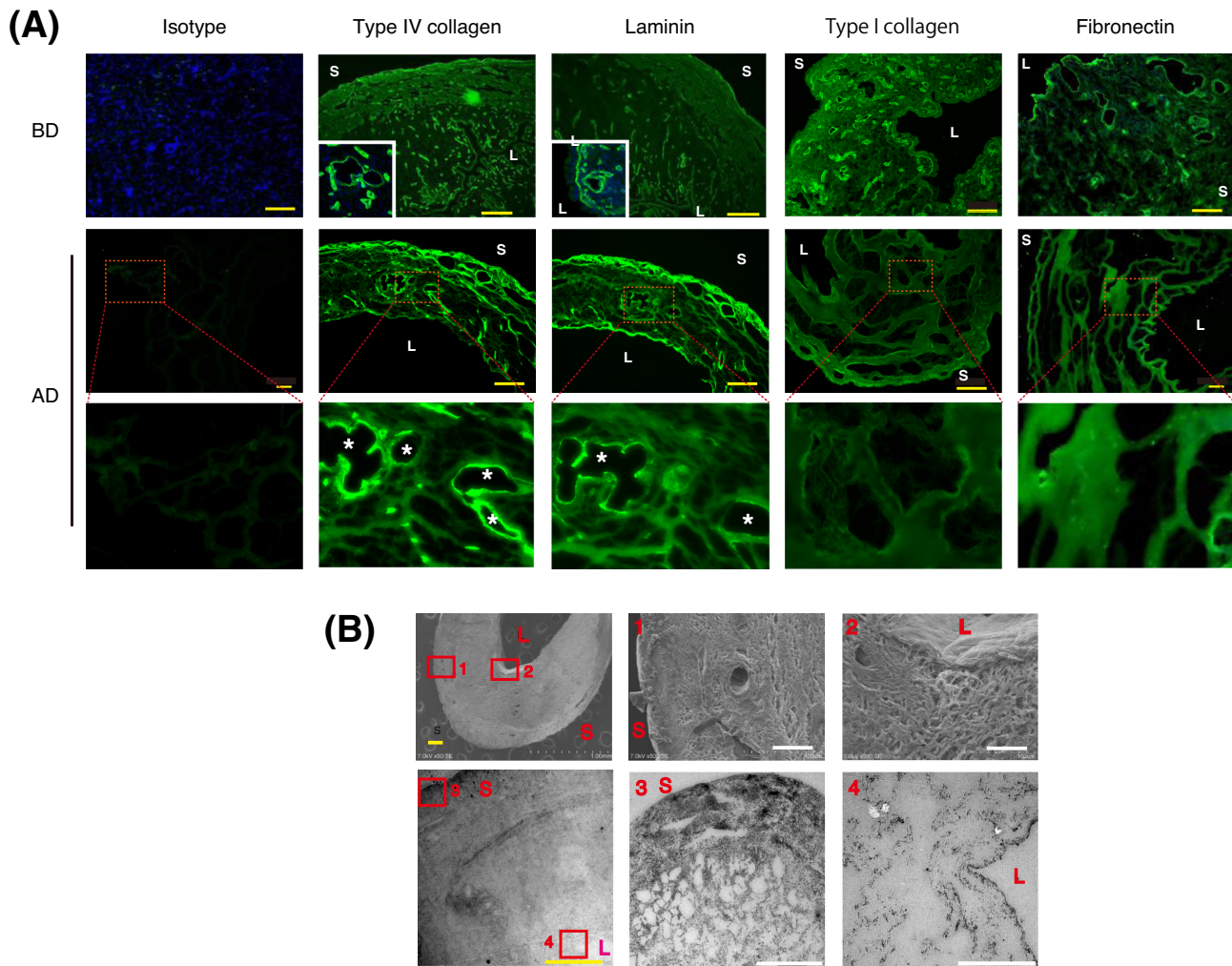
Figure 1. Retained components and preserved structure of the uterus after decellularization. (A) Immunofluorescent micrographs of rat uterus thin sections before (BD, upper four panels) and after (AD, lower four panels) decellularization using antibodies against extracellular matrix components as indicated. The insets show details of the staining patterns at higher magnification. Small red boxes delineate regions shown at higher magnification in the adjacent panel as indicated. Asterisks indicate glandular- and vascular-like structures. S, serosal side; L, luminal side. Scale bars, 200 μm. (B) Transmission electron micrographs (upper three panels) and scanning electron micrographs (lower three panels) of DUS. Small red boxes mark regions shown at higher magnification in the adjacent panels as indicated by the corresponding number. S, serosal side; L, luminal side. Yellow scale bars, 200 μm; white scale bars, 50 μm.

absent after decellularization (Supplementary Figure S1B and C, AD) as determined by histological and immunofluorescence studies (Supplementary Figure S1B and C, respectively).

In contrast, ECM proteins, including types I and IV collagen, laminin, and fibronectin that were present in the uterus before decellularization remained after decellularization (Figure 1A, BD and AD). Type IV collagen was highly expressed in the myometrium, vasculature, and the luminal and glandular epithelial basement membranes, with the most intensive labeling in the vasculature, whereas it was only weakly detectable in interstitial areas of the endometrium and absent in luminal and glandular epithelial cells (Figure 1A, inset). Laminin was also detected in endothelial layers around the blood vessels and in the luminal and glandular epithelial layers (Figure 1A, inset). The staining patterns of these uterine ECM proteins before decellularization were similar to those previously reported [25–28]. Notably, the distribution of these ECM proteins was not even throughout the uterus. Instead, the proteins were rather more dense on the serosal side than the luminal side before decellularization (Figure 1A and BD). The distribution patterns of these ECM proteins, in particular type IV collagen and laminin, were

preserved, at least in part, after decellularization (Figure 1A and AD). The intense staining signals of type IV collagen and laminin were detected at the putative basal layers of glandular- and vascular-like structures (Figure 1A, asterisks). Considering the preservation of the gradient and basal-like layer-selective distribution of those uterine ECM proteins after decellularization, we further examined the ultrastructure of the DUS using SEM and TEM. The ultrastructural analysis revealed that the ECM-based tissue skeleton together with the vascular and glandular architectures was retained in the DUS and that the density of the tissue skeleton was higher on the serosal side than the luminal side (Figure 1B).

Effect of the initial DUS orientation on the subsequent regeneration and tissue topology of the rat uterus

A DUS patch can repair and regenerate the rat uterus both structurally and functionally when placed on the defective uterine area [11, 12, 15]. An underlying ECM together with an acellular, perfusable vascular architecture preserved by the DUS is believed to be responsible for the appropriate regeneration of the uterus when a
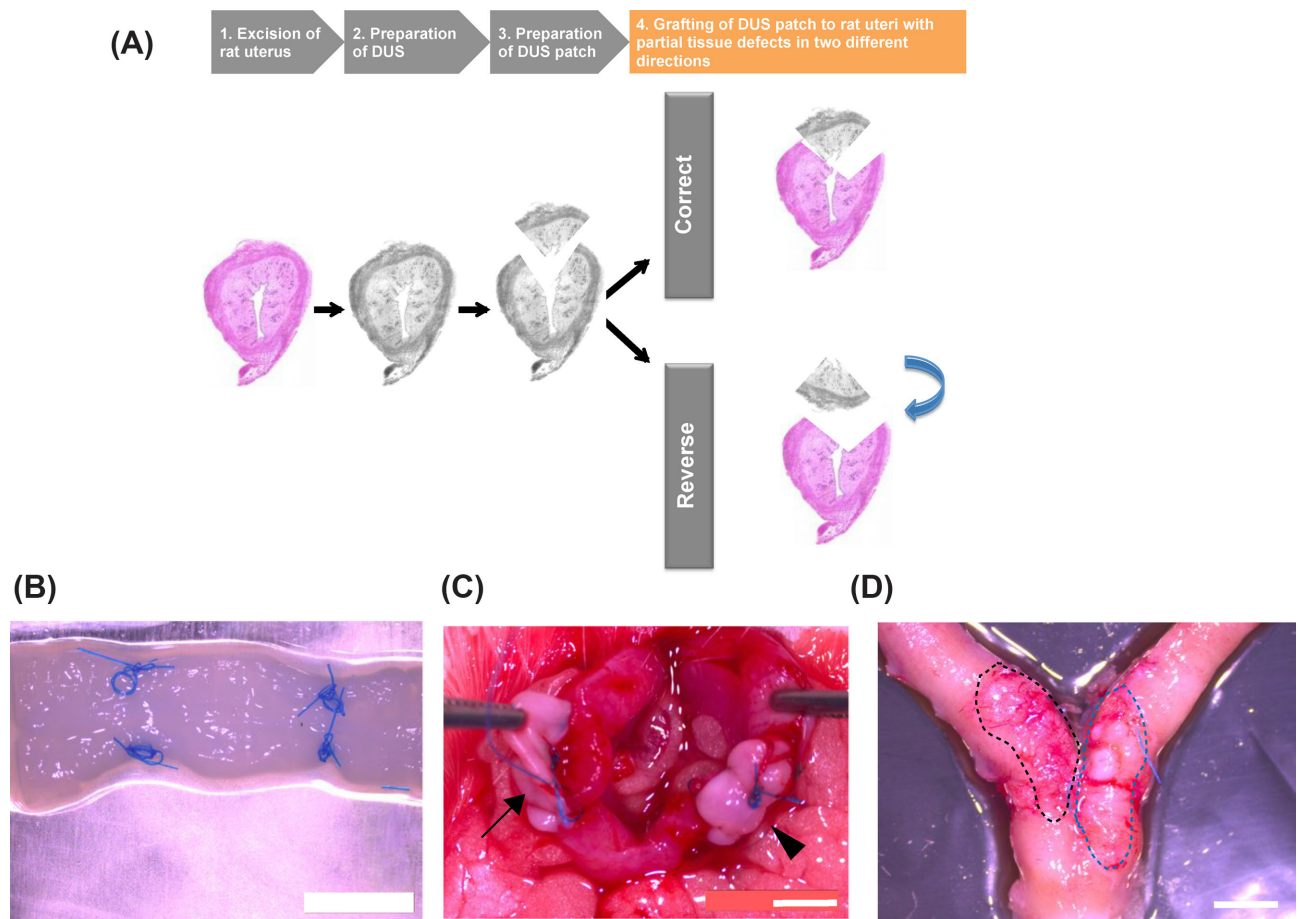
Figure 2. Placement of DUS patches onto partially defective rat uteri in correct and incorrect orientations. (A) Schema of the experimental protocol. DUS patches were prepared and preserved in PBS at 4°C. In replacement experiments, both uterine horns of the rat were segmentally excised at the anti-mesometrial side (AM). Subsequently, one horn was treated with a DUS patch placed onto the partially defective uterine area in the correct orientation, whereas the other horn was treated with a DUS patch in the reversed orientation. M, mesometrial side. (B) Marking of the lumen side of the DUS with 6-0 PROLENE sutures. Scale bar, 5 mm. C. Placement of DUS patches onto the partially defective area of the left uterine horn in the correct orientation (arrow) and onto that of the right horn in a reversed orientation (arrowhead). Note that the lumen side marked with 6-0 PROLENE suture is placed inside in the left horn (arrow) but outside in the right horn (arrowhead). The 6-0 PROLENE sutures were removed just before the completion of the replacement. Scale bar, 5 mm D. Macroscopic findings of the placement areas of the uterus 8 weeks after DUS patch placement in the correct and reversed orientations (black and blue dotted lines, respectively). Scale bar, 5 mm.

DUS is recellularized [10, 17–19]. To elucidate whether the ECM-based tissue skeleton in a DUS is responsible for the tissue polarity and architecture of a regenerated uterus, we placed DUS patches onto the partially defective uterine area not only in the correct orientation but also in a reversed orientation, in which the luminal side of the DUS was outside and the serosal side was inside (Figure 2A).

We marked the lumen side of the DUS patch with 6-0 PRO-LENE sutures (Figure 2B) and placed the marked DUS patches onto the partially defective area of the right uterine horn in the correct orientation and onto that of the left horn in a reversed orientation (Figure 2C). Macroscopically, 8 weeks after DUS placement, the uterine tissues were regenerated after DUS patches were placed in both the correct and reversed orientation (Figure 2D, dotted lines).

Microscopic analysis of the regenerated uteri using H&E and MT staining revealed that the areas in which the DUS were placed in correct or reversed orientations were well recellularized (Figure 3A, dotted lines). However, the linings of the smooth muscle layers were aberrant and partly disrupted (Figure 3A, red arrowhead). Furthermore, some gland-like structures were located far

from the luminal cavity, close to the serosal side and, intriguingly, outside the smooth muscle layer (Figure 3A, yellow arrowhead). The ectopic locations of some glands and the aberrant structure of the smooth muscle layer following placement of the DUS in the reverse orientation were further confirmed by immunofluorescence studies using antibodies against alpha-smooth muscle actin (uterine smooth muscle) and cytokeratin (luminal and glandular epithelium) (Figure 3B).

We conducted histologic examinations of the DUS-patched uteri. The tissues were classified into four categories by focusing on the structure of the smooth muscle layer and the location of the glands (Figure 4A). Categories included the following: normal (Type I), ectopic location of glands alone (Type II), irregular (tortuous and/or disrupted) architecture of smooth muscle layer alone (Type III), and mixture of Type II and Type III (Type IV). Type I designated a normal uterine horn, whereas either Type II, III, or IV indicated abnormal uterine horn histology (Figure 4A). In the 20 DUS patches that were oriented correctly, 14, 2, and 4 horns were classified into Types I, II, and III, respectively (Figure 4B). In contrast, of the 20 DUS that were oriented incorrectly, we found 6 Type I, 2 Type II, 5 Type
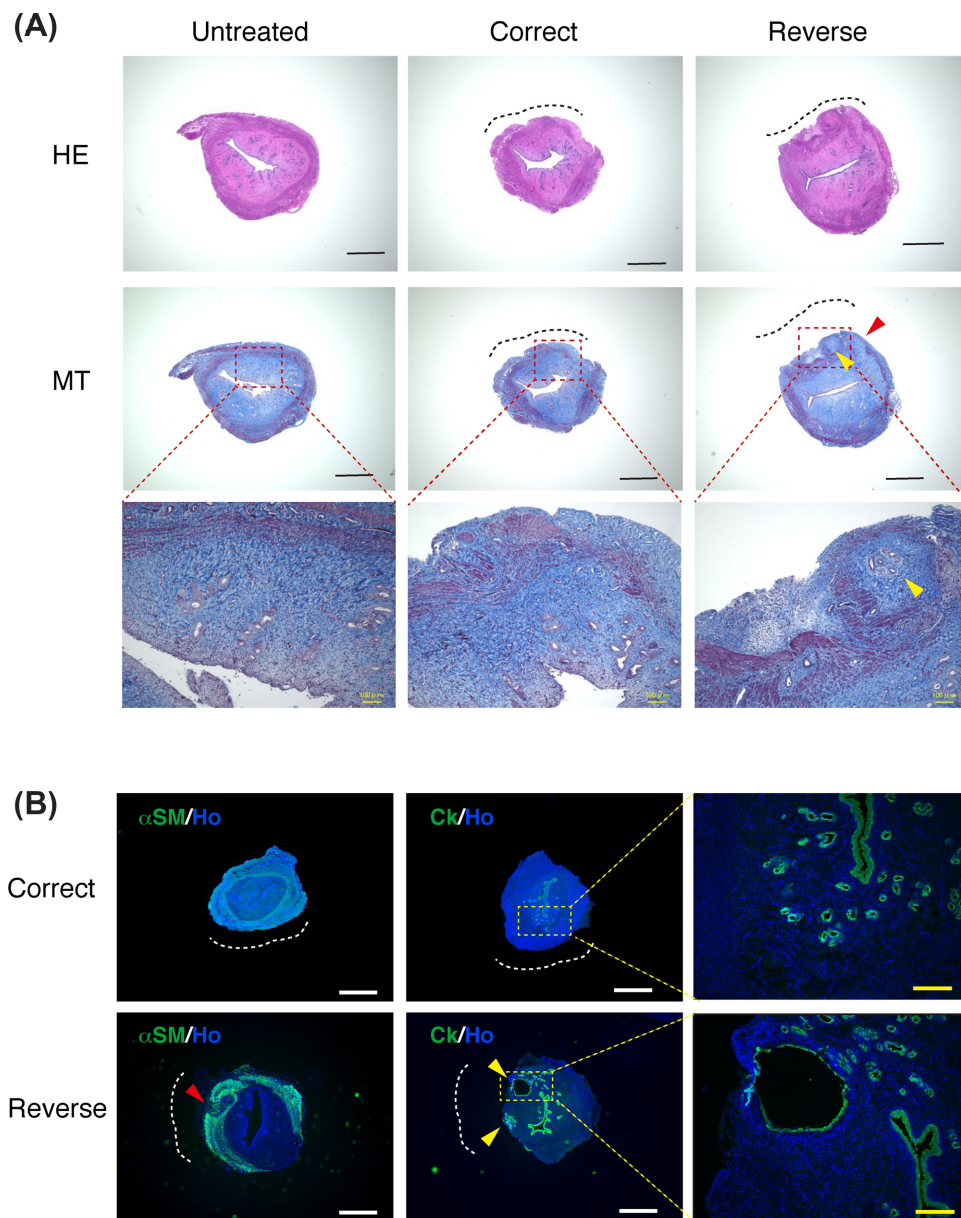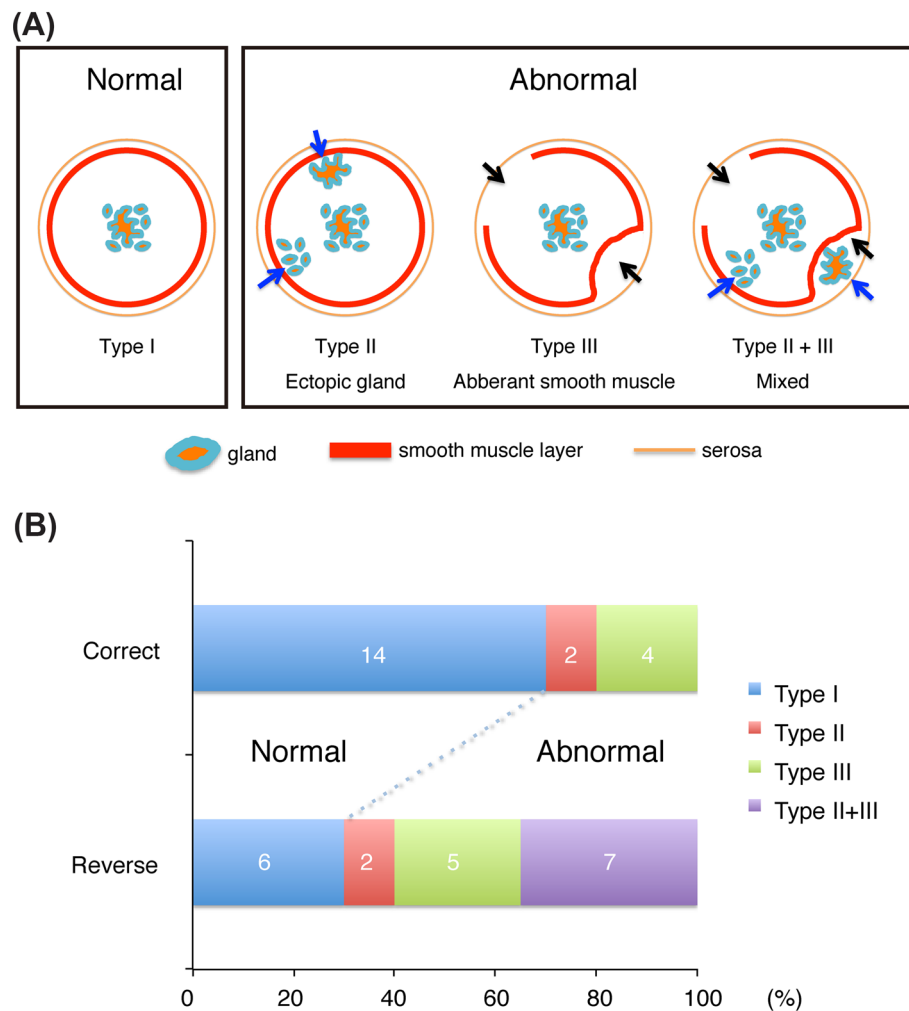
Figure 3. Tissue structures of the regenerated uteri after DUS placement in a correct or reversed orientation. (A) H&E staining (upper three panels) and MT staining (middle and lower three panels) of the rat uterine horns without (left two panels) and with DUS placed in the correct (middle two panels) or reversed (right two panels) orientation as indicated. Dotted lines indicate repair sites. Small boxes delineate regions shown at higher magnification in the adjacent panel as indicated. Note that the uterine horn with DUS placed in the reversed orientation showed a disruption of the smooth muscle layer and the ectopic location of glands (red arrowhead and yellow arrowheads, respectively). Scale bars, 1 mm. (B) Immunofluorescence staining of the rat uterine horn with a DUS patch placed in the correct or reversed orientation as indicated using antibodies against cytokeratin (Ck) and alpha-smooth muscle actin (αSM) followed by Hoechst (Ho) staining for visualization of nuclei. Dotted lines indicate repair sites. Small boxes mark regions shown at higher magnification in the adjacent panel as indicated. Note that the uterine horn with DUS placed in the reversed orientation showed aberrant smooth muscle structure and the ectopic location of glands (red arrowhead and yellow arrowheads, respectively). White scale bars, 1 mm; yellow scale bars, 200 μm.

III, and 7 Type IV (Figure 4B). Thus, abnormal uterine horns were significantly more common when the DUS patches were placed in the reversed orientation than in the control group (70% vs. 30%, $P < 0.05$).

In spite of the more frequent disruption of tissue topology in uterine horns treated with improperly oriented DUS patches, the distribution patterns of several ECM proteins were not apparently different. However, the ectopic glands were positive for type I collagen (Supplementary Figure S2). Also, the expression levels of *Esr1* and *Pgr* mRNAs were similar among untreated, correct, and reversed groups (Supplementary Figure S3). The intensities and patterns of ESR1 and PGR expression were also similar among the untreated, correct, and reversed DUS-situated groups (Supplementary Figure S4). These results raised the possibility that uterine horns repaired with an improperly oriented DUS might be able to respond to estrogen and progesterone and thereby achieve and maintain pregnancy.

Figure 4. Aberrant structures of the uterine horn regenerated after proper orientation or disoriented DUS placement. (A) Classification of regenerated uterine horns based on tissue structure. Each type is defined as indicated and described in the Results section. Blue arrows indicate the ectopic location of glands (type II), and black arrows indicate irregular (tortuous and/or disrupted) architecture of the smooth muscle layer (type III). The left upper two panels in (B) are classified as Type I. The lower left and middle panels in (B) are classified as Type III and Type II, respectively. (B) The proportion of each type of regenerated uterine horns patched with a DUS in the correct or reversed orientation. Abnormal uterine horns were more frequently observed in the reversed group than in the correctly oriented group (70% vs. 30%, $P < 0.05$).

Effect of DUS orientation on achieving and maintaining pregnancy

We tested the potential of rat uterine horns to support pregnancy following their repair with correctly oriented or reverse-oriented DUS patches. The females were mated with male SD rats 8 weeks after DUS placement. Fertilization was confirmed by the presence of a vaginal plug. Rats were euthanized 20 days after the appearance of the vaginal plug, and uterine horns were harvested and assessed for the number of fetuses per horn, fetal weight, histological, and immunofluorescence characteristics.

The uterine horns treated with DUS patches placed in either the correct or reversed orientation were able to achieve pregnancy (Figure 5A). The number of fetuses per uterine horn was, however, less in the DUS-treated horns than in the untreated horns, a difference that was significant (Figure 5B). There was no significant difference in the number of fetuses per uterine horn between the correct and reverse groups (Figure 5B). The pregnancy rate per uterine horn and the average weight of fetuses were similar among the three groups (Figure 5C and D). Furthermore, the microscopic appearance of uteroplacental units was similar among the three groups (Figure 5E).

In both humans and rodents, uterine endometrial stromal cells exhibit decidualization during pregnancy [18]. Particularly in rats, decidual cells are characterized by their capacity to produce decidua-specific proteins, such as desmin [25, 26]. Immunofluorescence studies showed an increased expression of desmin in stromal cells in the untreated and correct groups of DUS-treated animals, indicating decidualization of the endometrium in these groups (Supplementary Figure S5). By contrast, the expression of desmin was absent in the stroma of non-pregnant untreated rats, whereas the myometrium is strongly positive for desmin (Supplementary Figure S5).

Preparation and characterization of rat DSIS

Here, we demonstrated that the placement of a DUS patch in a reversed orientation resulted in the disruption of tissue topology more severely than the placement of a patch in the correct
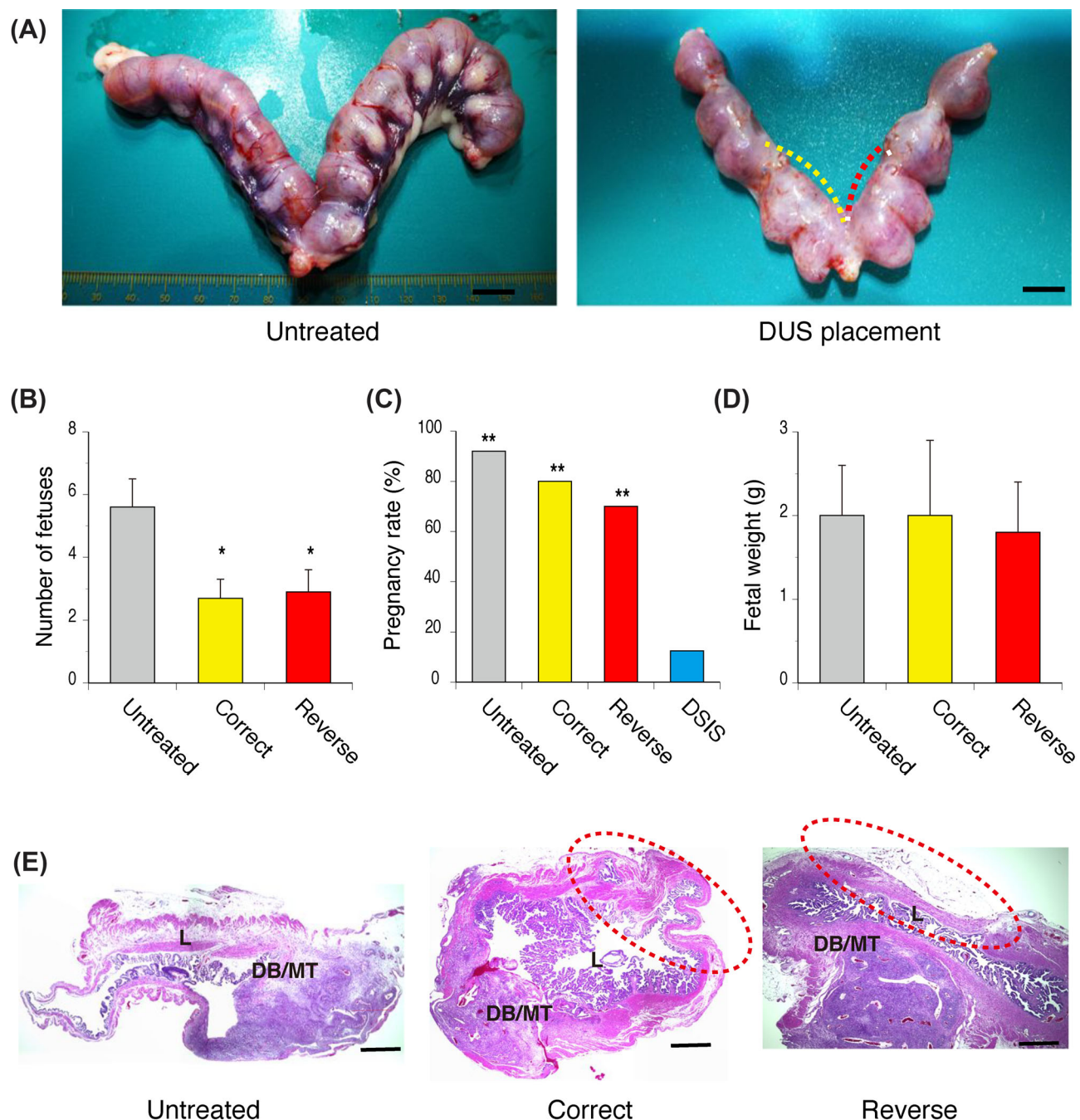
Figure 5. Achievement of pregnancies in rat uterine horns regenerated by properly oriented or disoriented DUS placement. (A) Gross findings of pregnant uteri untreated or treated with DUS patches placed in the correct or reversed orientation 20 days after mating. The portions treated with a DUS in the correct or reversed orientations are indicated by yellow and red dotted lines, respectively. Rats were mated 8 weeks after DUS placement. Scale bars, 10 mm. (B–D) Number of fetuses (B), pregnancy rate (C), and fetal weight (D) in rats treated as indicated 20 days after mating with male rats. Bars indicate the mean + SEM (B and D) or the percentage (C). *, $P < 0.05$ vs. untreated; **, $P < 0.05$, vs. DSIS (decellularized small intestine scaffold). (E) H&E staining of uteroplacental units in rats untreated or treated with DUS patches in the correct or reverse orientation 20 days after mating as indicated. The portions treated with DUS patches in either orientation are indicated by red dotted lines. DB/MT, decidua basalis/mesometrial triangle; L, labyrinth. Scale bars, 1 mm.

orientation. Those results suggested that the improper orientation of DUS ECM proteins can disturb in vivo recellularization even when their amounts and components are similar. We therefore asked whether a DS obtained from a non-uterine site would negatively affect in vivo recellularization. We utilized DS prepared from the small intestine (DSIS) as a representative test material because the small intestine is structurally and functionally distinct from the uterus although both are luminal organs.

We prepared DSIS from rats through soaking and shaking with SDS as described in the Materials and methods section. Figure 6A showed the gross findings of the small intestine before and after decellularization (BD and AD, respectively). Both cell nuclei and
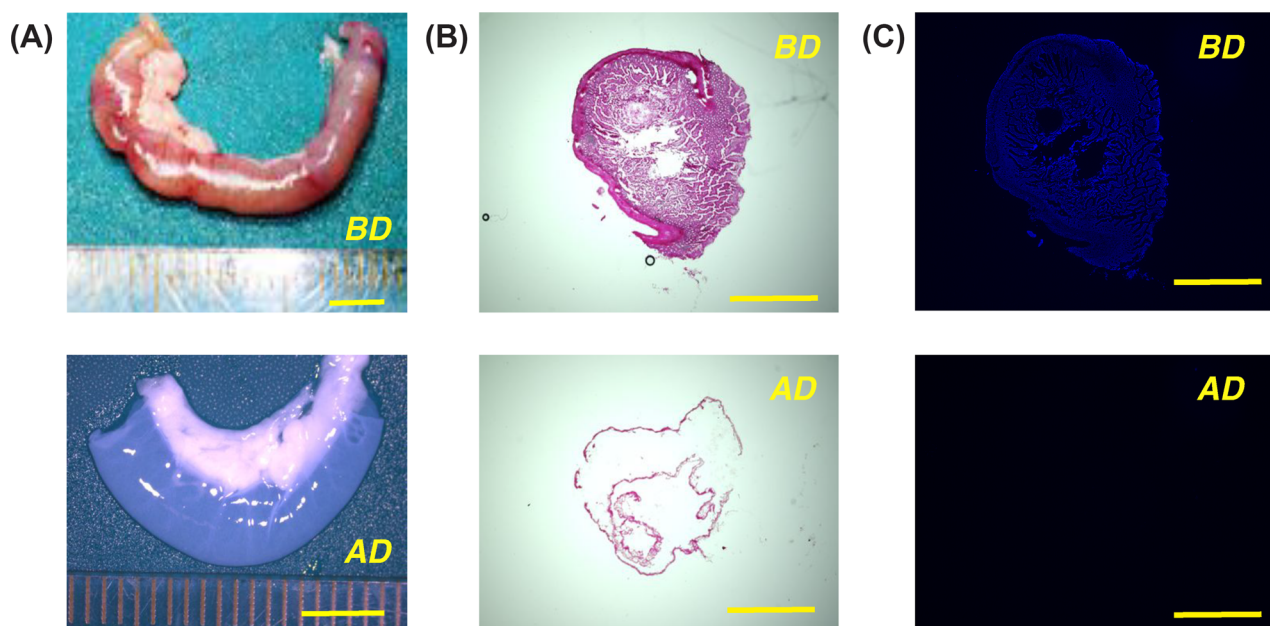
Figure 6. Decellularization of rat small intestine (A) Macroscopic appearance of rat small intestines before and after decellularization (BD and AD, respectively). Scale bars, 5 mm. (B). H&E-stained micrographs of rat small intestine thin sections before and after decellularization (BD and AD, respectively). Scale bars, 1 mm. (C) Nuclear staining of rat small intestine thin sections by Hoechst dye before and after decellularization (BD and AD, respectively). Note that intact cells were removed together with loss of Hoechst-positive nuclei (blue). Scale bars, 1 mm.

cytoplasmic components present in the rat small intestine before decellularization (Figure 6B and C, BD) were lost after decellularization (Figure 6B and C, AD) as determined by H&E staining and immunofluorescence (Figure 6B and C, respectively). In contrast, ECM proteins, including types I, IV, and V collagen, laminin, fibronectin, and vitronectin, that were present in the small intestine before decellularization, remained at least in part, after decellularization (Supplementary Figure S6). In particular, type IV collagen and laminin were better preserved in the mucosa compared to other ECM proteins (Supplementary Figure S6). Like the native uterus and DUS, the ECM proteins were denser on the serosal side than the luminal side before and also after decellularization (Supplementary Figure S6).

Effect of DSIS on the regeneration and tissue topology of the rat uterus

We placed DSIS patches onto partially defective areas of both rat uterine horns (Figure 7A, dotted lines). Eight weeks after placement of the DSIS patches, the uterine tissues appeared to be regenerated at both horns (Figure 7B, dotted lines). Microscopic analysis of the regenerated uteri using H&E and MT staining revealed that the DSIS-patched area was recellularized. However, the uterine wall was very thin and lacked a smooth muscle layer (Figure 7C, dotted lines). This uterus was classified as Type III according to the classification previously described (Figure 4A). In the eight DSIS-patched uterine horns, we did not observe a Type I structure (normal) or a Type II structure. Instead, we found five Type IIIs, and three Type IVs. Thus, the DSIS group exhibited abnormal morphologies (Types III and IV) significantly more frequently than did the group treated with DUS patches in the correct orientation (100% vs. 30%, $P < 0.005$) and more frequently (but not significantly, 100% vs. 70%, $P = 0.141$) than the group treated with a DUS patch in the reversed orientation (Figure 4B and Supplementary Figure S7).
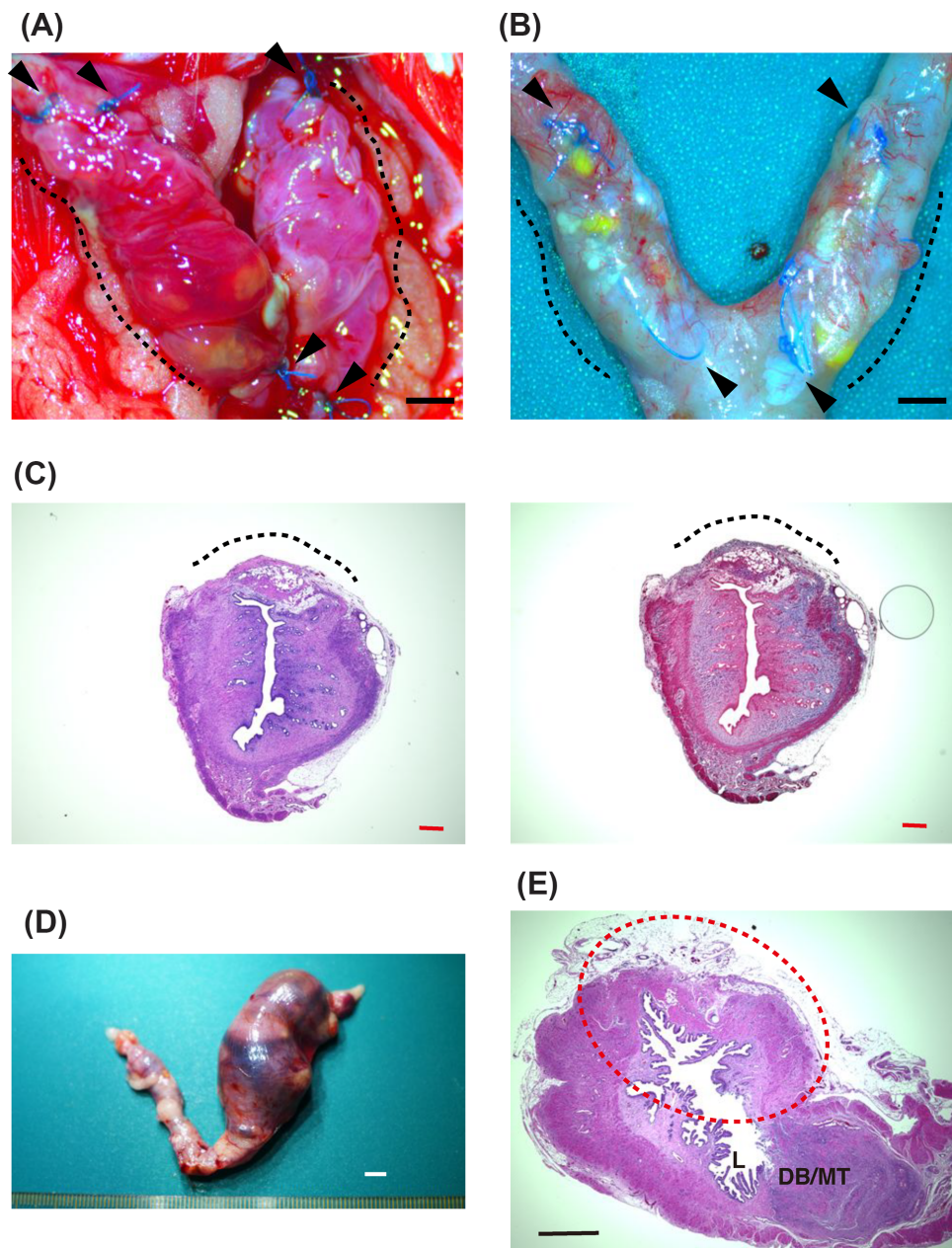
Effect of DSIS patches on pregnancy

We tested the potential of the DSIS-driven regenerated uterine horns to achieve pregnancy. Thus, rats with uterine horns treated with a DSIS were mated with male SD rats 8 weeks after DSIS placement. Rats were euthanized 20 days after the appearance of the vaginal plug, and uterine horns were harvested to assess the number of fetuses per horn, fetal weight, and histological appearance. Among the eight DSIS-placed uterine horns, only one horn achieved pregnancy apart from the DSIS placement area (Figure 7D). The microscopic appearance of the uteroplacental unit was almost normal (Figure 7E). Thus, the number of fetuses per uterine horn was significantly lower in the DSIS-treated horns than untreated horns and DUS-patched horns (Figure 5C).

Discussion

We previously reported that the DUS preserves ECM and 3D architecture and that it has the potential to partially regenerate the functional uterus in rats [11]. Based on the previous results, we asked how DUS-preserving ECM and 3D architecture guided uterine regeneration. In this study, we investigated the effect of DUS orientation to address this question and found that placing DUS patches in uterine horns in the reversed orientation led to the development of an aberrant tissue structure. However, the pregnancy potential of the horns was comparable to that of uterine horns treated with scaffolds placed in the correct orientation and showed a normal tissue structure. The area that we partially excised and treated with a DUS patch was the anti-mesometrial side of the uterus (Figure 3A). We chose this strategy because the mesometrial side is vascular-rich and even partial excision leads to massive and uncontrollable bleeding. In rodents, implantation and placentation take place on the mesometrial side, not the anti-mesometrial side of the uterus [29]. Collectively, these observations indicate that the tissue integrity and

Figure 7. Non-pregnant and pregnant rat uteri regenerated after placement of decellularized small intestine scaffolds (DSIS). (A) Placement of DSIS patches onto the partially defective area of both uterine horns (black dotted lines). Note that the luminal side was placed inside and fixed by blue 6-0 PROLENE sutures (arrowheads). Scale bar, 2 mm. (B) Macroscopic findings of the placement areas of the uterus 8 weeks after DSIS patch placement (black dotted lines). Arrowheads, blue 6-0 PROLENE sutures. Scale bar, 2 mm. (C) H&E staining (left panel) and MT staining (right) of the rat uteri regenerated after DSIS placement. Dotted lines indicate repair sites. Scale bars, 100 μm. (D) Gross findings of pregnant uteri placed with DSIS on both horns 20 days after mating. Note that there were no conceptuses in the left horn and only one conceptus in the right horn. Rats were mated 8 weeks after DSIS placement. Scale bar, 5 mm. (E) H&E staining of pregnant uteri treated with DSIS placement 20 days after mating. Dotted lines indicate repair sites. DB/MT, decidua basalis/mesometrial triangle; L, labyrinth. Scale bar, 1 mm.

function of an aberrantly structured uterus is sufficiently robust to support the conceptus as a capsule. However, it remains to be elucidated whether the uterine region regenerated by a reverse-oriented DUS is able to directly support an embryo's implantation and placentation. In the DSIS, the distribution, constitution, and amount of ECM proteins differed from those of the DUS and did not support regeneration of a normally structured uterus that could support pregnancy.

The versatile functions of the ECM depend on its diverse physical, biochemical, and biomechanical properties, including anchorage to the basement, dual modulator as a barrier and guide for cell migration, signal reservoir, low affinity signal co-receptor for some growth factors, signal presenter to determine the orientation of cell-cell communication, functional fragment derivatives, such as matrix metalloproteinases and provider of biomechanical forces [18, 19]. Among the various roles of ECM, the regulation of cell migration

from the surrounding tissue is very important for the recellularization of an acellular ECM scaffold and subsequent regeneration of the target tissue in vivo.

It has been reported that the placement of a collagen scaffold loaded with bone marrow mesenchymal stem cells or collagen-binding human basic fibroblast growth factor can successfully regenerate a functional rat uterus [30–32]. Those observations suggest that a simple and homogenous ECM scaffold without any material polarities assists tissue self-organization and reconstruction through the action of migrating or pre-loaded cells. A scaffold with a more complicated structure, like a DS patch, can also promote tissue self-organization and reconstruction when placed in the correct orientation. However, when placed in the wrong orientation, a DS patch may disturb the self-regenerative and self-organizing abilities of migrating uterine cells, resulting in a topological change of regenerated tissues/organs. In agreement, the change of tissue topology was more evident with a DSIS patch. These results collectively suggest that cell migration and positioning are primarily dependent on the status of the ECM and skeletonized architecture rather than the self-regenerative and self-organizing activities of uterine cells.

A recent study employed a DUS-driven uterine regeneration model in mice. It showed that uterine luminal epithelial cells (designated as flat cells) rapidly migrated onto the DUSs and formed a normal uterine epithelial layer within a week [33]. Furthermore, they claimed that the flat cells formed a gland-like structure in the transplanted DUS on day 3, indicating that migration and invagination of luminal epithelial cells are responsible for the regeneration of the glandular epithelium [33]. Acellular architecture of the luminal epithelial layer of a DUS patch became continuous with the neighboring epithelium when the DUS was placed in the correct orientation. This placement enabled neighboring epithelial cells to move and migrate onto the DUS horizontally along the epithelial architecture. However, when the patch was placed in the reversed orientation, the epithelial architecture of the DUS was discontinuous with the surrounding luminal and glandular epithelium. Nevertheless, we found that gland-like structures were generated in DUS patches placed in an incorrect orientation. Intriguingly, these gland-like structures were located distant from the luminal epithelium and rather close to the serosa (Figure 3). Thus, epithelial cells of the ectopic glands are unlikely to directly migrate along the epithelial layer architecture from the luminal and glandular epithelium. These findings collectively suggest that there may be alternative mechanism(s) for the regeneration of glands. One such alternative mechanism is that cells migrating into and recellularizing the stroma (perhaps mature stromal cells, or endometrial stem/progenitor cells or glandular progeny) may give rise to the glandular epithelium through a mesenchymal–epithelial transition or differentiation. In support of this mechanism, it is believed that bone marrow-derived cells migrate into the endometrium and thereafter generate not only endometrial stromal cells but also glandular cells [34, 35]. In this context, skeletonized glandular architecture containing gland-specific ECMs present in a DUS may act as a possible micro-environmental trigger or driver to transform the migrating stromal cells into glandular cells. In support of our idea, it is generally accepted that ECM controls mammary gland formation through ECM-driven guidance of mammary stem cell fate [36]. In agreement with our idea, a DSIS patch did not support the generation of glandular structures even when migrating cells recellularized the DSIS because it lacked the skeletonized endometrial glandular architecture. Alternatively, ECM components of the DSIS may initially block or mislead the migration of competent cells from neighboring uterine tissue into DSIS. Although we did not compare the tissue weights and ECM contents between DSIS and DUS, it appeared that the DSIS was thinner and much less dense than the DUS, which might result in a poorer regeneration at the defective area of the uterus. Alternatively, the DSIS might need more than 56 days (8 weeks) to complete uterine regeneration. Indeed, Li et al. and Ding et al. assessed the collagen scaffold-driven regeneration of the rat uterus 30–90 days after repair by collagen scaffolds [30, 31]. In this study, we assessed the regeneration of the DSIS-patched uterus only 8 weeks after DSIS patch placement; therefore, we cannot rule out possible delaying effects of DSIS.

In this study, placement of the DUS in the uterine horns in a reversed orientation generally led to ectopic location of glands and aberrant microscopic structure of the smooth muscle layer. These microscopic findings are rather similar to those of rodent models of adenomyosis in which neonatal administration of tamoxifen induces adenomyotic lesions mainly characterized by extensive downgrowth, i.e., peripheral and ectopic location of endometrial glands and stroma into the thickened, abnormal myometrium with disorganized fascicles of smooth muscle and increased interstitial collagen deposition [37, 38]. Thus, disoriented DUS placement offers a way to develop a rodent model of uterine malformation, reminiscent of diseases such as adenomyosis. It is tempting to speculate that disoriented ECM production and location may primarily contribute to adenomyosis and other uterine disorders.

The ultimate goal of this analysis of uterine regeneration using DUS patches in animals [11–16] is to apply these procedures and techniques to humans in clinical settings and to regenerate a whole human uterus in vivo and in vitro. However, in the near term, we hope to use the DUS patch methodology to treat partial defects of the uterus due to myomectomy for uterine fibroids, adenomyomectomy for uterine adenomyosis, and conization or trachelectomy for uterine cervical cancer [9]. The results of the present study substantiate the importance of a DUS patch's orientation in the development and establishment of normal tissue topology.

Conclusions

This report describes the importance of the orientation of DUS patches for uterine regeneration in rats. Our study found that placing DUS patches in uterine horns in the reversed orientation led to the development of an aberrant tissue structure, suggesting that the orientation of DUS-preserving ECM and 3D architecture affects the structure of the regenerated uterus. Using the DUS in the correct orientation is preferable when clinically applied. Although the fertility potential is not immediately affected, the disoriented DUS may deteriorate the tissue topology leading to structural disease of the uterus.

Supplementary data

Supplementary data are available at *BIOLRE* online.

Supplemental Figure S1. Decellularization of the rat uterus. (A) Macroscopic appearance of rat uteri before and after decellularization (BD and AD, respectively). Scale bars, 1 cm. (B) Hematoxylin and eosin (H&E)-stained micrographs of rat uterus thin sections before and after decellularization (BD and AD, respectively). Scale bars, 100 μm. (C) Nuclear staining of rat uterus thin sections by Hoechst dye before and after decellularization (BD and AD, respectively). Note that intact cells were removed together with loss of Hoechst-positive nuclei (blue). Scale bars, 200 μm.

Supplemental Figure S2. Immunofluorescence of ECM using indicated antibodies with Hoechst dye for nuclear staining of rat uterus and DUS. Note that the epithelium of the ectopic gland (EG) was positive for type I collagen (red arrowheads), whereas the epithelium of the normal gland was negative in both correct and reversed groups (yellow arrowheads). Scale bars, 200 μm.

Supplemental Figure S3. Expression of *Esr1* and *Pgr* mRNAs in the untreated or DUS-placed rat uteri. Relative mRNA expression levels of *Esr1* (A) and *Pgr* (B) in uterine horns untreated or treated with DUS placement in the correct or reversed orientation as determined by real-time PCR. Note that there were no significant differences in the relative expression of *Esr1* and *Pgr* mRNAs among the three groups.

Supplemental Figure S4. Expression of ESR1 and PGR in the untreated or DUS-treated rat uteri. Immunofluorescence of the uterine horns that were untreated or treated with DUS patches in the correct or reversed orientation using antibodies against ESR1 (A) and PGR (B). Bars, 100 μm.

Supplemental Figure S5. Expression of desmin, a decidual marker, in untreated or DUS-patched pregnant and non-pregnant rat uteri. (A) Immunofluorescence of decidua in the untreated or DUS-patched pregnant and non-pregnant rat uterine horns stained with an antibody against desmin together with Hoechst DNA dye. D: decidua, Myo: myometrium, St: stroma. Scale bars, 200 μm. (B) Quantification of fluorescence intensity of desmin signals. Bars indicate the mean + SEM of the signals. P: pregnant, NP: non-pregnant, C: Correctly oriented DUS placement, U: untreated, R: reversely orientated DUS placement, D: decidua, St: stroma, Myo: myometrium. *, $P < 0.05$ vs. the first bar (the decidua of correctly DUS-patched pregnant uterus stained with an isotype antibody); **, $P < 0.05$ vs. the second bar (the stroma of untreated non-pregnant uterus stained with an antibody against desmin).

Supplemental Figure S6. Immunofluorescence of ECM of rat small intestine and DSIS. Immunofluorescence of ECM using antibodies as indicated together with Hoechst for nuclear staining in rat small intestine and DSIS. S, serosal side; L, luminal side. Scale bar, 200 μm.

Supplemental Figure S7. The proportion of each type of uterine horn regenerated after DUS placement in the correct or reversed orientation or after DSIS placement. Each type is defined as described in the Results section and Figure 4. No uterine horn with a type I structure (normal) was observed in the DSIS group, indicating that the DSIS group exhibited abnormal structure significantly more frequently than the correct DUS group ($P < 0.005$) and more frequently but not significant ($P = 0.141$) than the reversed DUS group.

Acknowledgments

References

1. Goldfarb JM, Austin C, Peskin B, Lisbona H, Desai N, de Mola JR. Fifteen years experience with an in-vitro fertilization surrogate gestational pregnancy programme. *Hum Reprod* 2000; **15**:1075–1078.
2. Brannstrom M, Johannesson L, Bokstrom H, Kvarnstrom N, Molne J, Dahm-Kahler P, Enskog A, Milenkovic M, Ekberg J, Diaz-Garcia C, Gabel M, Hanafy A et al. Livebirth after uterus transplantation. *Lancet North Am Ed* 2015; **385**:607–616.
3. Brannstrom M. Womb transplants with live births: an update and the future. *Expert Opin Biol Ther* 2017; **17**:1105–1112.
4. Shenfield F, Pennings G, Cohen J, Devroey P, de Wert G, Tarlatzis B. ESHRE Task Force on Ethics and Law 10: surrogacy. *Hum Reprod* 2005; **20**:2705–2707.
5. Nakash A, Herdiman J. Surrogacy. *J Obstet Gynaecol* 2007; **27**:246–251.
6. Testa G, Johannesson L. The ethical challenges of uterus transplantation. *Curr Opin Organ Transplant* 2017; **22**:593–597.
7. Alghrani A. Uterus transplantation: does procreative liberty encompass a right to gestate? *J Law BioSci* 2016; **3**:636–641.
8. Hellstrom M, Bandstein S, Brannstrom M. Uterine tissue engineering and the future of uterus transplantation. *Ann Biomed Eng* 2017; **45**:1718–1730.
9. Cervello I, Santamaria X, Miyazaki K, Maruyama T, Simon C. Cell therapy and tissue engineering from and toward the Uterus. *Semin Reprod Med* 2015; **33**:366–372.
10. Song JJ, Ott HC. Organ engineering based on decellularized matrix scaffolds. *Trends Mol Med* 2011; **17**:424–432.
11. Miyazaki K, Maruyama T. Partial regeneration and reconstruction of the rat uterus through recellularization of a decellularized uterine matrix. *Biomaterials* 2014; **35**:8791–8800.
12. Santoso EG, Yoshida K, Hirota Y, Aizawa M, Yoshino O, Kishida A, Osuga Y, Saito S, Ushida T, Furukawa KS. Application of detergents or high hydrostatic pressure as decellularization processes in uterine tissues and their subsequent effects on in vivo uterine regeneration in murine models. *PLoS One* 2014; **9**:e103201.
13. Campo H, Baptista PM, Lopez-Perez N, Faus A, Cervello I, Simon C. De- and recellularization of the pig uterus: a bioengineering pilot study. *Biol Reprod* 2017; **96**:34–45.
14. Hellstrom M, El-Akouri RR, Sihlbom C, Olsson BM, Lengqvist J, Backdahl H, Johansson BR, Olausson M, Sumitran-Holgersson S, Brannstrom M. Towards the development of a bioengineered uterus: comparison of different protocols for rat uterus decellularization. *Acta Biomater* 2014; **10**:5034–5042.
15. Hellstrom M, Moreno-Moya JM, Bandstein S, Bom E, Akouri RR, Miyazaki K, Maruyama T, Brannstrom M. Bioengineered uterine tissue supports pregnancy in a rat model. *Fertil Steril* 2016; **106**:487–496.
16. Padma AM, Tiemann TT, Alshaikh AB, Akouri R, Song MJ, Hellstrom M. *Protocols for Rat Uterus Isolation and Decellularization: Applications for Uterus Tissue Engineering and 3D Cell Culturing*. New York: Humana Press; 2017.
17. Agmon G, Christman KL. Controlling stem cell behavior with decellularized extracellular matrix scaffolds. *Curr Opin Solid State Mater Sci* 2016; **20**:193–201.
18. Gattazzo F, Urciuolo A, Bonaldo P. Extracellular matrix: a dynamic microenvironment for stem cell niche. *Biochim Biophys Acta - Gen Subj* 2014; **1840**:2506–2519.
19. Lu P, Weaver VM, Werb Z. The extracellular matrix: a dynamic niche in cancer progression. *J Cell Biol* 2012; **196**:395–406.
20. Gurung S, Deane JA, Masuda H, Maruyama T, Gargett CE. Stem cells in endometrial physiology. *Semin Reprod Med* 2015; **33**:326–332.
21. Ono M, Maruyama T. Stem cells in myometrial physiology. *Semin Reprod Med* 2015; **33**:350–356.
22. Masuda H, Maruyama T, Hiratsu E, Yamane J, Iwanami A, Nagashima T, Ono M, Miyoshi H, Okano HJ, Ito M, Tamaoki N, Nomura T et al. Noninvasive and real-time assessment of reconstructed functional human endometrium in NOD/SCID/ Formula immunodeficient mice. *Proc Natl Acad Sci USA* 2007; **104**:1925–1930.
23. Masuda H, Matsuzaki Y, Hiratsu E, Ono M, Nagashima T, Kajitani T, Arase T, Oda H, Uchida H, Asada H, Ito M, Yoshimura Y et al. Stem cell-like properties of the endometrial side population: implication in endometrial regeneration. *PLoS One* 2010; **5**:e10387.
24. Miyazaki K, Maruyama T, Masuda H, Yamasaki A, Uchida S, Oda H, Uchida H, Yoshimura Y. Stem cell-like differentiation potentials of endometrial side population cells as revealed by a newly developed in vivo endometrial stem cell assay. *PLoS One* 2012; **7**:e50749.

25. Glasser SR, Lampelo S, Munir MI, Julian J. Expression of desmin, laminin and fibronectin during in situ differentiation (decidualization) of rat uterine stromal cells. *Differentiation* 1987; **35**:132–142.

26. Korgun ET, Cayli S, Asar M, Demir R. Distribution of laminin, vimentin and desmin in the rat uterus during initial stages of implantation. *J Mol Hist* 2007; **38**:253–260.

27. Diao H, Aplin JD, Xiao S, Chun J, Li Z, Chen S, Ye X. Altered spatiotemporal expression of collagen types I, III, IV, and VI in Lpar3-deficient peri-implantation mouse uterus. *Biol Reprod* 2011; **84**:255–265.

28. Campo H, Cervello I, Simon C. Bioengineering the uterus: an overview of recent advances and future perspectives in reproductive medicine. *Ann Biomed Eng* 2017; **45**:1710–1717.

29. Lim HJ, Wang H. Uterine disorders and pregnancy complications: insights from mouse models. *J Clin Invest* 2010; **120**:1004–1015.

30. Li X, Sun H, Lin N, Hou X, Wang J, Zhou B, Xu P, Xiao Z, Chen B, Dai J, Hu Y. Regeneration of uterine horns in rats by collagen scaffolds loaded with collagen-binding human basic fibroblast growth factor. *Biomaterials* 2011; **32**:8172–8181.

31. Ding L, Li X, Sun H, Su J, Lin N, Peault B, Song T, Yang J, Dai J, Hu Y. Transplantation of bone marrow mesenchymal stem cells on collagen scaffolds for the functional regeneration of injured rat uterus. *Biomaterials* 2014; **35**:4888–4900.

32. Song T, Zhao X, Sun H, Li X, Lin N, Ding L, Dai J, Hu Y. Regeneration of uterine horns in rats using collagen scaffolds loaded with human embryonic stem cell-derived endometrium-like cells. *Tissue Eng Part A* 2015; **21**:353–361.

33. Hiraoka T, Hirota Y, Saito-Fujita T, Matsuo M, Egashira M, Matsumoto L, Haraguchi H, Dey SK, Furukawa KS, Fujii T, Osuga Y. STAT3 accelerates uterine epithelial regeneration in a mouse model of decellularized uterine matrix transplantation. *JCI Insight* 2016; **1**:e87591.

34. Taylor HS. Endometrial cells derived from donor stem cells in bone marrow transplant recipients. *JAMA* 2004; **292**:81–85.

35. Bratincsak A, Brownstein MJ, Cassiani-Ingoni R, Pastorino S, Szalayova I, Toth ZE, Key S, Nemeth K, Pickel J, Mezey E. CD45-positive blood cells give rise to uterine epithelial cells in mice. *Stem Cells* 2007; **25**:2820–2826.

36. Ghajar CM, Bissell MJ. Extracellular matrix control of mammary gland morphogenesis and tumorigenesis: insights from imaging. *Histochem Cell Biol* 2008; **130**:1105–1118.

37. Parrott E, Butterworth M, Green A, White IN, Greaves P. Adenomyosis–a result of disordered stromal differentiation. *Am J Pathol* 2001; **159**:623–630.

38. Green AR, Styles JA, Parrott EL, Gray D, Edwards RE, Smith AG, Gant TW, Greaves P, Al-Azzawi F, White IN. Neonatal tamoxifen treatment of mice leads to adenomyosis but not uterine cancer. *Exp Toxicol Pathol* 2005; **56**:255–263.